Research Article

Study on Mechanical Behavior of Fully Encased Composite Slender Columns with High-Strength Concrete Using FEM Simulation

Getinet Melesse,[1] Samuel Jima,[1] Tegegn Asale,[1] Yayesew Moges,[2] and Hibretu Kaske Kassa [ID] [2]

[1]*School of Civil Engineering, Institute of Technology, Arbaminch University, Arba Minch, Ethiopia*
[2]*Department of Civil Engineering, Debre Tabor University, South Gondar, Ethiopia*

Correspondence should be addressed to Hibretu Kaske Kassa; hibretuk2015@gmail.com

The most common types of composite columns used in high-rise structures are concrete-filled steel tubes (CFSTs) and concrete-encased steel (CES) that are either entirely or partially encased in concrete. The attempt of this study is to develop a suitable constitutive model addressing the behavior of fully encased composite slender columns with high-strength concrete subjected to axial loading. The nonlinear finite element (FE) package ABAQUS version 6.14-2 is used to study the response of fully encased composite (FEC) slender columns. The finite element analysis (FEA) results are validated with experimental data extracted from previous experiments. Then, the parametric study is conducted on rectangular FEC columns with different shapes of encased steel encasements to investigate the axial load-carrying capacities, axial deformation, ductility, load-deformation behavior, and confinement of FEC columns. The governing parameters for the current study are the high strength of concrete (90 MPa, 100 MPa, and 120 MPa), shapes of encased steel sections (circular, I-shaped, and rectangular steel encasements), and spacing of tie bars (50 mm, 100 mm and 150 mm). 6–21% of load increment is observed by changing the concrete compressive strength. A comparison is also made between the results of reinforced concrete and FEC slender columns and 2–11% of load increment is recorded by changing the shape of structural steel and keeping other parameters constant. The results of calibrated finite element models revealed that closely spaced tie bars resulted in a good ductility of FEC column with high-strength concrete (HSC). Significant enhancements in the axial load capacity are observed in the case of FEC slender columns than in RC slender columns of the same size and shape. Ductility and residual strength after the failure of FEC columns are also observed to increase significantly with the adoption of tubular structural steel sections. However, increasing the concrete strength results in the reduction of this ductility.

1. Introduction

Modern skyscrapers, also known as high-rise buildings, tall structures, and towers, are what catches our attention the most when we see a lot of structures today, whether they are large or small, old or new, simple or complex. These structures are made of extraordinary advances in science and engineering technology. For architects and engineers, the urban population boom poses a significant difficulty because the land is at a premium. Vertical development, also referred to as a vertical city because of its capacity to provide more ground space and house more people in a given amount of space, is the solution to this kind of problem. However, doing so is becoming more expensive, so we need a framework that is more rigid and stable. Composite construction is a novel invention that was introduced to attain the stability, strength, and stiffness of the constructions. A composite structural member is made of two or more materials, each of which has unique features, joined together by a shear connection. One type of composite compression structural member is the composite column, which has a cross-section made of either concrete inside

a structural steel tube (concrete-filled steel tube or CFST) or structural steel inside concrete (concrete-encased steel or CES). For CES composites, fully encased composite (FEC) and partially encased composite (PEC) column sections are both available. The FEC column is the only one of these three parts that does not require any additional money for corrosion and fire protection because the steel portion is completely covered by concrete [1, 2]. Therefore, from the perspectives of strength, ductility, and economy, it may be the ideal option for tall constructions [3].

The CES composite column is chosen for the current study as a consequence. In reality, low-rise to high-rise buildings use CES composite columns. Under loading circumstances, concrete is prevented from excessively spalling by the rebar (main and tie bar). In order to create a stiff, more ductile, economical, and structurally sound component for building and bridge construction, embedded steel sections and reinforced concrete sections are used in combination as composite members. This is because of their interaction behavior [4–6].

Ethiopian cities are currently seeing an increase in the construction of high-rise buildings. High-strength materials are already being utilized in many regions of the world in CES composite columns of substantially loaded structures (high-rise buildings, long-span bridges, and offshore constructions) in order to reduce material consumption and improve the strength and performance of the structures. However, adopting strong materials is not a very common practice in Ethiopia. The ground floor columns in medium-rise structures (20–30 stories high) constructed of normal strength concrete (NSC) may have a diameter of more than one meter. Imagine there is no space on the ground level if a very tall skyscraper was to be built using NSC [3]. As a result, the use of high-strength concrete (HSC) in the construction of tall buildings produces materials that are strong, compact, and long-lasting. In general, CES columns with NSC have ductility and can reach the axial capacity indicated by the code. However, CES columns with HSC exhibit brittle behavior. Because of this brittleness, the concrete roof of the HSC always breaks off suddenly and without warning, and the steel does not fully develop its plasticity. Axial load capacity is suddenly reduced as a result of this. Because of recent developments in concrete technology, concrete with a compressive strength of up to 100 MPa can now be manufactured commercially with a tolerable amount of variability using regular particles. These changes have prompted a rise in the usage of HSC globally [7, 8]. By minimizing the cross-sectional dimensions of the columns, the use of high-strength materials in composite columns increases the benefits of structural safety, economy, and space need.

By examining the impact of various parameters, this research study aims to provide an insight into the behavior of FEC thin columns with HSC under concentric axial stress. A significant amount of experimental and few numerical investigations was performed on the strength and failure modes of FEC columns under concentric and eccentric loading conditions. According to [6, 9–12], the failure mechanism of FEC columns with a slenderness ratio

of up to 25 is initiated by both crushing of concrete on the compression side and tensile damage of concrete on the tension side followed by the yielding of structural steel and longitudinal reinforcement. On the other hand, for columns with a large slenderness ratio (L/D > 25), the failure mode is only due to tensile damage of concrete and a flexural buckling of the column. It is necessary to investigate the effects of various parameters on the behavior of FEC slender columns, including the spacing between tie bars, the compressive strength of concrete (high and ultrahigh strength), and various shapes of encased steel sections (circular, rectangular, and I-shaped encasements). Designers and academics can utilize this to learn more about the structural behavior and failure modes of FEC slim columns with HSC [1, 2, 10]. As a result, the objective of this study is to carry out numerical analyses on FEC thin columns with HSC under axial concentric loading circumstances.

2. Materials and Methods

All simulations of fully encased composite (FEC) columns are carried out using ABAQUS/Standard [13], in order to accomplish the goal of this research. It can accurately describe the nonlinear behavior of steel reinforcing bars and concrete. The geometrical and material parameters of FE models as well as the characteristics of test specimens are described in the chapter's following section on finite element modeling.

2.1. Finite Element Modeling. Currently, computer-aided analysis of FEC columns using finite element methods is needed to augment experimental approaches, broaden our understanding of these columns' behavior, and better comprehend the effects of various factors on their strength and behavior. As a result, the goal of this research is to create a comprehensive 3D nonlinear FE model that can be used for a variety of parameters and to deliver precise simulations of the structural behavior and mechanisms of failure of FEC narrow columns subjected to concentric axial loadings. FEA permits direct modeling of the composite activity between steel and concrete components. However, the input parameters have a significant impact on how accurate the forecast is. The FE models are calibrated based on experimental results conducted by [6, 14]. Then, parametric investigations are conducted addressing the effects of various parameters such as the compressive strength of concrete, different shapes of encased steel sections, and spacing of tie bars in order to fully understand the behavior of FEC slender columns with HSC.

2.2. Geometrical Properties of the Finite Element Model. In the present study, the FE program [13] is used to develop a complete 3D nonlinear FE model to investigate the behavior of FEC slender columns with HSC. The columns comprise of three components, namely, concrete, structural steel, and rebar (main bars and tie bars).

TABLE 1: Mechanical properties of the structural steel and rebar as per [16, 17].

Materials	f_y (MPa)	f_u (MPa)	$E_{s/a}$ (GPa)	μ_s
Structural steel	355	457.95	210	
Main bars	460	541.65		0.3
Tie bars	500	581.25	200	

2.2.1. Elements Selection. To address these various issues, the CES composite column components are modeled utilizing a range of elements from the ABAQUS element library. These include shell, beam, truss, and connection elements as well as solid (continuum) elements. Typically, solid pieces are used to simulate the concrete. C3D4, C3D6, and C3D8R are the three most often utilized solid elements offered by [13] for modeling. Elements C3D4 and C3D6 did not adequately converge in comparison to C3D8R, necessitating the use of fine mesh. Consequently, creating fine meshes took a lot of time. Since it is determined to be the most suitable from both the accuracy and time-required viewpoints, element C3D8R is utilized to represent the concrete portion of FEC slim columns. Both the solid element C3D8R and the shell components S3 and S4R can be used to simulate the structural steel component of FEC slim columns. The solid element C3D8R has three translational degrees of freedom (DOFs) per node. However, in addition to the translational DOFs, the shell components S3 and S4R also include three rotating DOFs (a total of six-degrees of freedom per node). Combining solid element C3D8R (only for concrete) with shell element S4R (only for structural steel) may cause compatibility problems at the place where the two elements meet. For this reason, structural steel is also included in the FE analysis using the solid element C3D8R. So, with the exception of reinforcement bars, solid element C3D8R is used for all parts of FEC slender columns. Typically, two-node truss elements T3D2 are used to simulate the reinforcing bars.

2.2.2. Mesh Discretization. Since mesh size selection has a significant impact on the FEA outcomes in terms of time, convergence, and solution quality, it is necessary for FE modeling. Typically, findings from finer meshes are extremely accurate (converged). These little meshes demand a lot of computational time, though. Mesh dependency should not be disregarded as a result. In order to select an appropriate mesh that offers reliable results and requires less computational time, several columns are designed and tested using various mesh sizes. The same element type is used for all tests, and the comparison is between axial load capacity and axial deformation. Because of this, it is preferable to use 40 mm mesh, which provides the optimum fit, but avoids using too much time.

2.2.3. Modeling of Steel-Concrete Interactions. The finite element's component parts are individually modeled and assembled as an assembly. Then, for modeling steel-concrete composite columns, the appropriate constraints and contact interactions between rebar (longitudinal and tie bars), structural steel, and concrete are described. This study uses
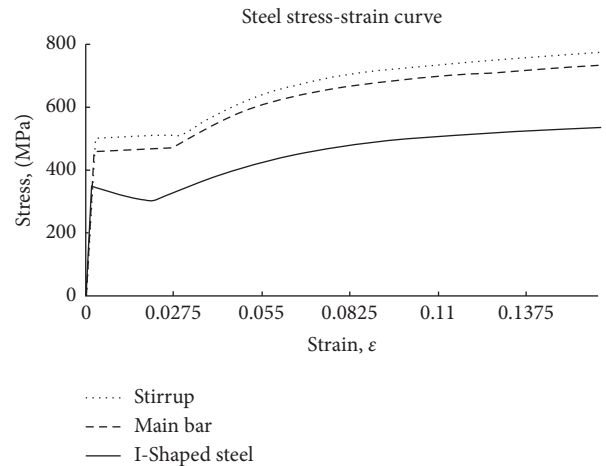

FIGURE 1: Stress-strain model for structural steel sections and reinforcements [16, 17].

the ABAQUS embedded region constraint option to model the bond behavior between structural steel and concrete. In the concrete, which serves as the host region, the structural steel is positioned as the embedding region. The nodes lose their translational degrees of freedom when the embedded elements are located within the host region, at which point they are referred to as embedded nodes. The response of the host elements thus limits the translational movements of the embedded parts. Since embedding rebar into concrete cannot accurately imitate its true behavior, the tie constraint option in ABAQUS is thought to be the best way to obtain good bond behavior between the contact interfaces of concrete and rebar [15]. For this technique, the master and slave surfaces must be specified. Generally speaking, the ABAQUS manual advises choosing the master and slave surfaces based on the material's rigidity as well as how soft or firm it is. Additionally, the stiffer material is chosen as a master surface while the less stiff material is chosen as a slave surface. The harder material is chosen as a master surface while the softer material is chosen as a slave surface. The concrete surfaces that surround the rebar are referred to as the master surface, while the surfaces of the rebar itself are referred to as slave surfaces. Then, the assigned tie constraint method fuses together the master and slave surfaces so that relative motion between the two surfaces cannot occur.

2.2.4. End Boundary Conditions. The FE model's end boundary conditions are established in a way that they are consistent with the experimental setup. The test column specimens were typically put into a testing device and the load was given directly to them, according to the published

TABLE 2: Summary of mechanical properties of the concrete.

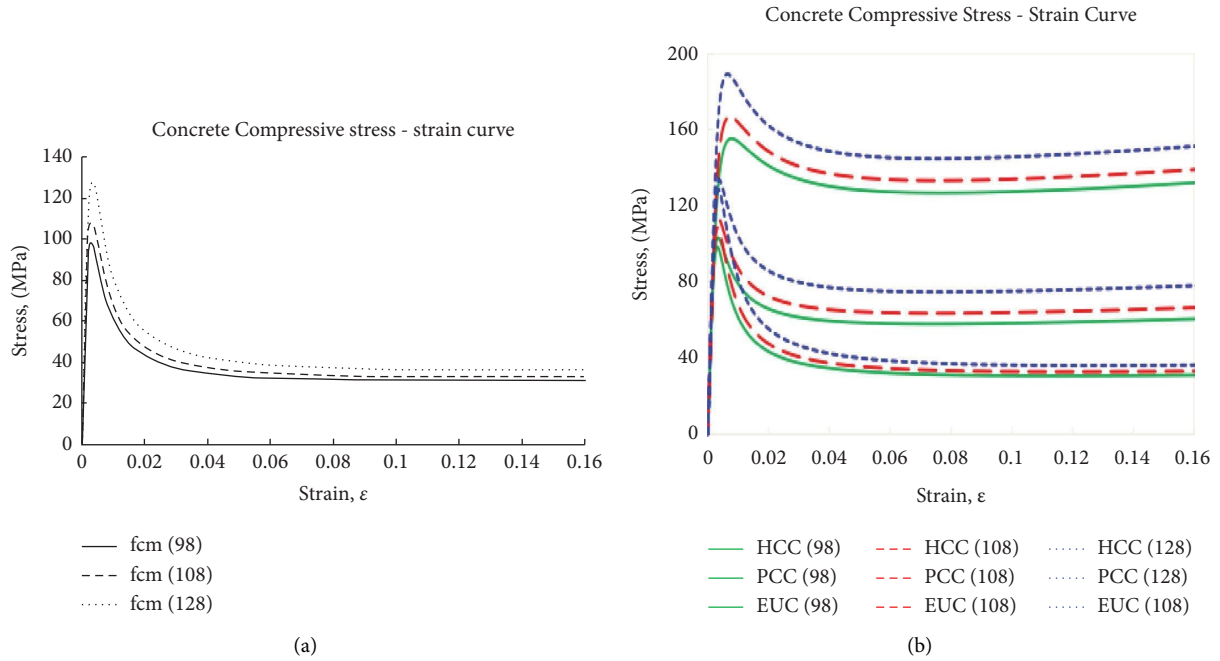| Materials	f_{ck} (MPa)	f_{cm} (MPa)	f_{ctm} (MPa)	E_{cm} (GPa)	μ_c
Concrete	90/105	98/115	5.045/5.355	43.631/45.775	0.2
	100/115	108/125	5.232/5.518	44.921/46.935	
	120/140	128/150	5.564/5.878	47.27/49.574	

FIGURE 2: Stress-strain curves for uniaxial (a) unconfined concrete compression and (b) confined concrete compression.

TABLE 3: Geometrical properties of column specimens.

Column	Length	Steel plate size	Main bar	Stirrups
$(B \times D)$ (mm)	L (mm)	$(h \times b_f \times t_w x \times t_f)/(D \times t)$ (mm)		
33×250	9000	—	4-Ø 12 mm	Ø8@50 mm
		Circ-steel pipe (150×6)	4-Ø 12 mm	
300×250	9000	Rect-$75 \times 62 \times 12 \times 12$	4-Ø 12 mm	Ø8@50 mm
		IPE200-$200 \times 100 \times 8.5 \times 5.6$	4-Ø 12 mm	
300×250	9000	—	4-Ø 12 mm	Ø8@50 mm

TABLE 4: Material properties of column specimens for the current study [6, 14].

	Concrete	Structural steel	Main bar	Tie bar
Compressive stress (F_{ck})	90–120 MPa			
Yield stress (F_y)	—	355 MPa	460 MPa	500 MPa
Ultimate stress (F_u)	—	457.95 MPa	541.65 MPa	581.25 MPa
Modulus of elasticity (E)	43.6305–47.27 GPa	210 GPa	200 GPa	200 GPa
Poison's ratio (v)	0.2	0.3	0.3	0.3
Yield strain (ε_y)	0	0.00169	0.0023	0.0025
Ultimate strain (ε_u)	0.0035	0.1551	0.1748	0.175

literature. To reduce the impact of the end conditions of the columns, the loading end plates are not included in the FE models in this thesis. Instead, the top and bottom surfaces of the core element are bound by two rigid body constraints with reference nodes (tie nodes or pin nodes). The load eccentricity is equal to the distance between the rigid body's reference point and the section's center. The rigid body's reference point and the section's center, however, coincide under conditions of concentric loading. Only the vertical restraint at the reference point on the top surface of the column is released to apply the axial compression load or displacement at that point, with the degree of freedom (DOF) at the base of the column being fully restrained in translations and rotations.
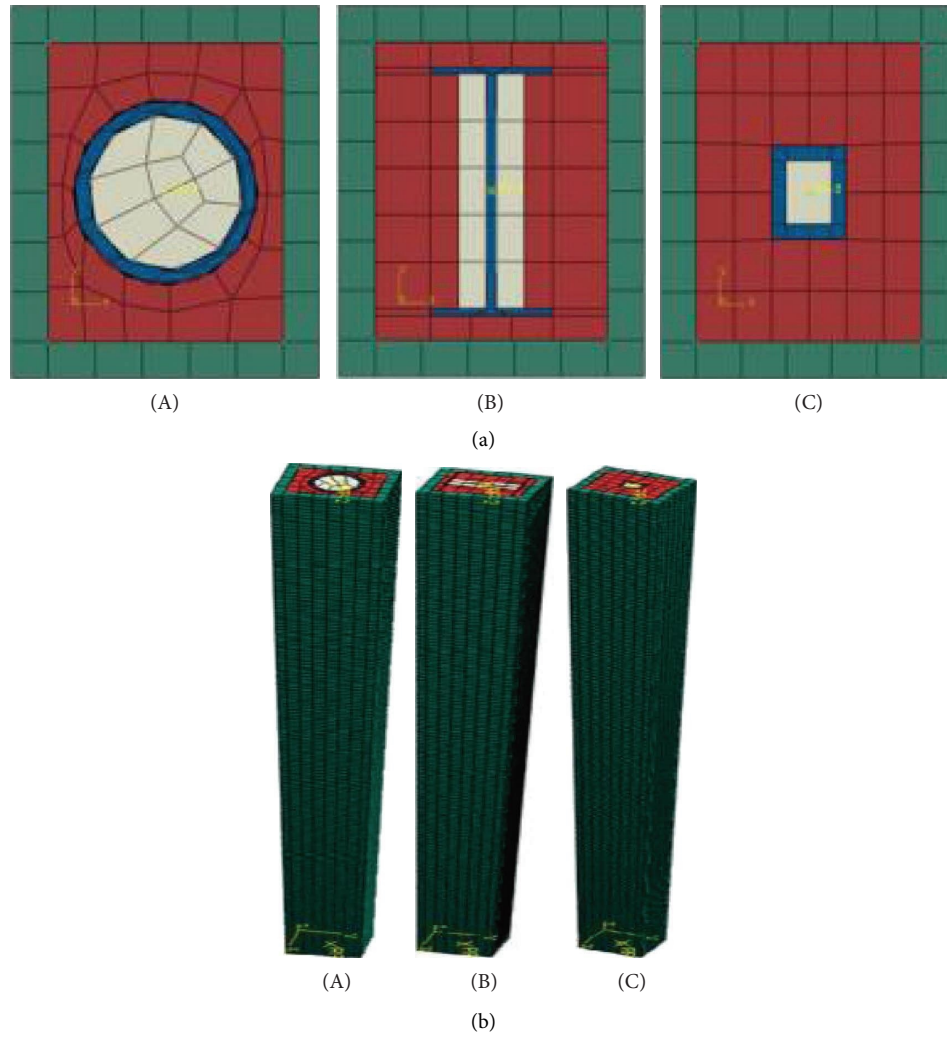
Figure 3: Geometry of FEC column specimens. (a) Plan view of (A) circular, (B) I-shaped, and (C) rectangular steel encasements for FEC column and (b) 3D View of (A) circular, (B) I-shaped, and (C) rectangular steel encasements for FEC columns.

Table 5: Specimens for effects of concrete compressive strength.

Column type	Column ID	$D \times B \times L$ (m)	Structural steel	S (mm)	F_y (MPa)	F_{ck} (MPa)
RCC	RHC1S1	$0.3 \times 0.25 \times 9$	—	100	—	90
	RHC2S1					100
	RHC3S1					120
FECC-C	CSHC1S1	$0.3 \times 0.25 \times 9$	Circular	100	355	90
	CSHC2S1					100
	CSHC3S1					120
FECC-I	ISHC1S1	$0.3 \times 0.25 \times 9$	I-shaped	100	355	90
	ISHC2S1					100
	ISHC3S1					120
FECC-R	RSHC1S1	$0.3 \times 0.25 \times 9$	Rectangular	100	355	90
	RSHC2S1					100
	RSHC3S1					120

TABLE 6: Specimens for effects of structural steel encasements.

Group	Column ID	$D \times B \times L$ (m)	S (mm)	F_{ck} (MPa)	F_y (MPa)	Structural steel	S (mm)
Group 1	Control-RHC1 HC1CS HC1IS HC1RS	$0.3 \times 0.25 \times 9$	50	90	355	— Circular I-shaped Rectangular	100
Group 2	Control-RHC2 HC2CS HC2IS HC2RS	$0.3 \times 0.25 \times 9$	50	100		— Circular I-shaped Rectangular	100
Group 3	Control-RHC3 HC3CS HC3IS HC3RS	$0.3 \times 0.25 \times 9$	50	120	355	— Circular I-shaped Rectangular	100

TABLE 7: Specimens for effects of tie bar spacing (s).

Column type	Column ID	$D \times B \times L$ (m)	F_{ck} (MPa)	S (mm)	Column ID	Column type
FECC-C	CSHC1s1 CSHC1s2 CSHC1s3	$0.3 \times 0.25 \times 9$	90	100 150 50	ISHC1s1 ISHC1s2 ISHC1s3	FECC-I
	CSHC2s1 CSHC2s2 CSHC2s3	$0.3 \times 0.25 \times 9$	100	100 150 50	ISHC2s1 ISHC2s2 ISHC2s3	
	CSHC3s1 CSHC3s2 CSHC3s3	$0.3 \times 0.25 \times 9$	120	100 150 50	ISHC2s1 ISHC2s2 ISHC2s3	
FECC-R	RSHC1s1 RSHC1s2 RSHC1s3	$0.3 \times 0.25 \times 9$	90			
	RSHC2s1 RSHC2s2 RSHC2s3	$0.3 \times 0.25 \times 9$	100			
	RSHC3s1 RSHC3s2 RSHC3s3	$0.3 \times 0.25 \times 9$	120			

TABLE 8: Geometrical properties of selected FEC test columns for validation.

References	Column ID	Dimensions		Reinforcements		Structural steel	
		$B \times D$ (mm)	L (mm)	Main bar	Tie bar	$h \times b \times t_f / D \times t$ (mm)	Shape
[4]	A1	180×160	3500	4-Ø12 mm	Ø8@150 mm	$100 \times 68 \times 4.5 \times 7.6$	I
[14]	C7	200×200	1400	4-Ø12 mm	Ø8@100 mm	100×3.5	Circular
	C9	200×200	1400	4-Ø12 mm	Ø8@100 mm	No. 10	I
[6]	S690-C90-SP60-H	260×260	600	8-Ø13 mm	Ø10@60 mm	$160 \times 160 \times 10 \times 18$	H

2.2.5. Load Application and Numerical Solution Strategy.
Both the load control technique and displacement control technique can be used to apply an axial load. It is not possible to acquire a displacement with regard to the peak load when the load is applied as a point load. However, if a point displacement is used, it is simple to determine the peak load and the related displacements, and the behavior after the postpeak load softens. As a result, in this study, the axial load is applied through the top rigid body reference node using the displacement control approach, and the nonlinear numerical equilibrium equations are solved using the Newton–Raphson iterative solution method.

2.3. Material Properties of the Finite Element Modeling.
Due to their nonlinear features, materials are exceedingly difficult to model in computer programs and require a lot of information on how they behave. The next sections provide detailed descriptions of HSC, structural steel, and rebar (main bars and tie bars) used in FEC thin columns, as well as information on their mechanical characteristics and stress-strain relationships.

2.3.1. Steel Material Properties for FE Modeling. Rebar (primary bars and tie bars) and structural steel exhibit comparable stress-strain behavior. They behave as linear

TABLE 9: Material properties of selected FEC test columns for validation.

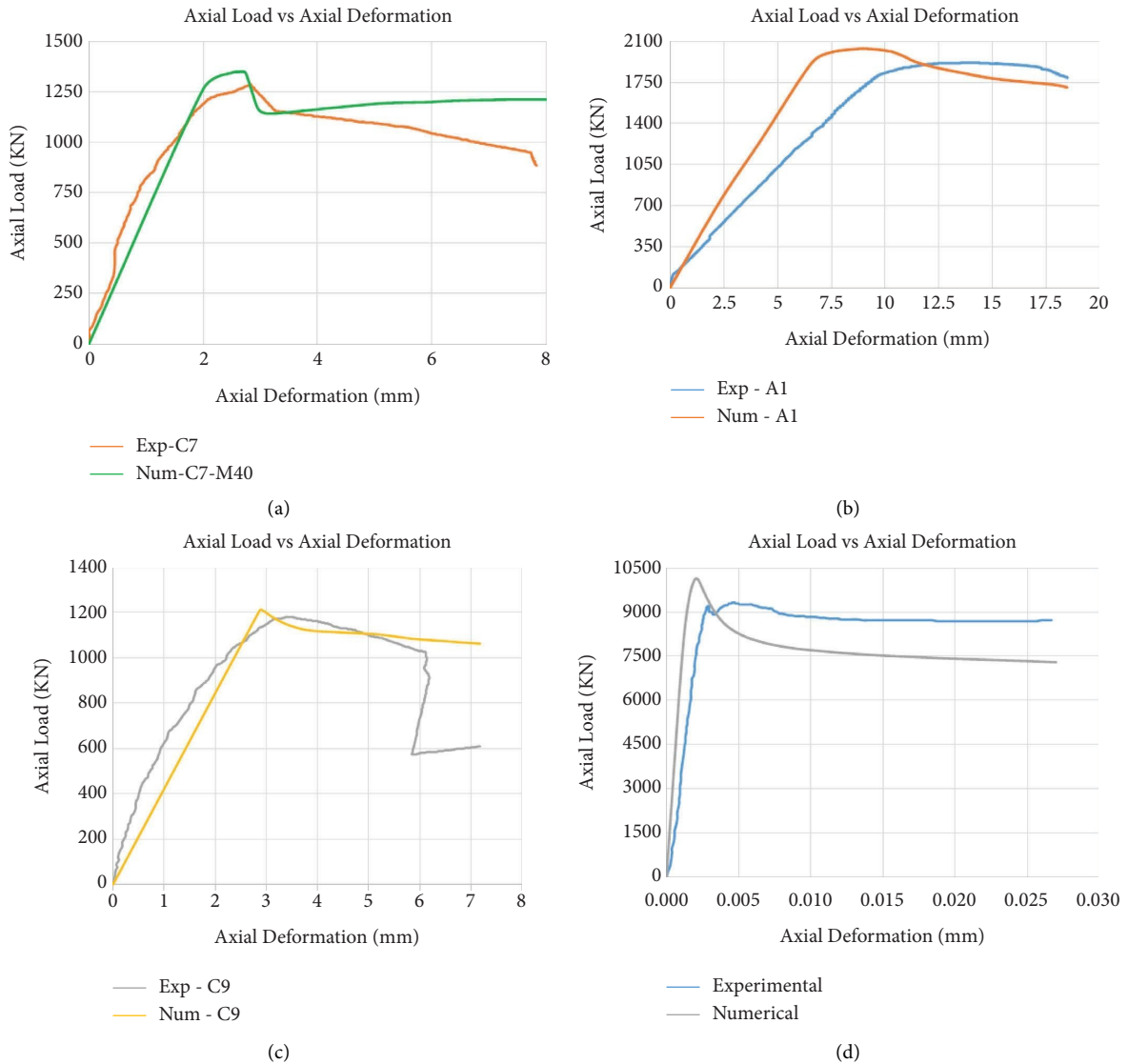| References	Column ID	Concrete			Structural steel		Reinforcement			
		f_{cm} (MPa)	E_c (GPa)	ν	F_y (MPa)	ν	F_y (MPa)	F_y (MPa)	E_s (GPa)	ν
[4]	A1	65.6	33.79	0.2	379	0.3	358		224/205.8	0.3
[14]	C7	31.7	31.10	0.2	240	0.3	400	320	200	0.3
	C9	31.1	30.92	0.2	240	0.3	400	320	200	0.3
[6]	S690-C90-SP60-H	94.6	43.17	0.2	739/887	0.3	578	510	200	0.3

FIGURE 4: Axial load vs. axial deformation curve for (a) A1 [4]; (b) C7 [14]; (c) C9 [14]; (d) S690-C90-SP60-H [6].
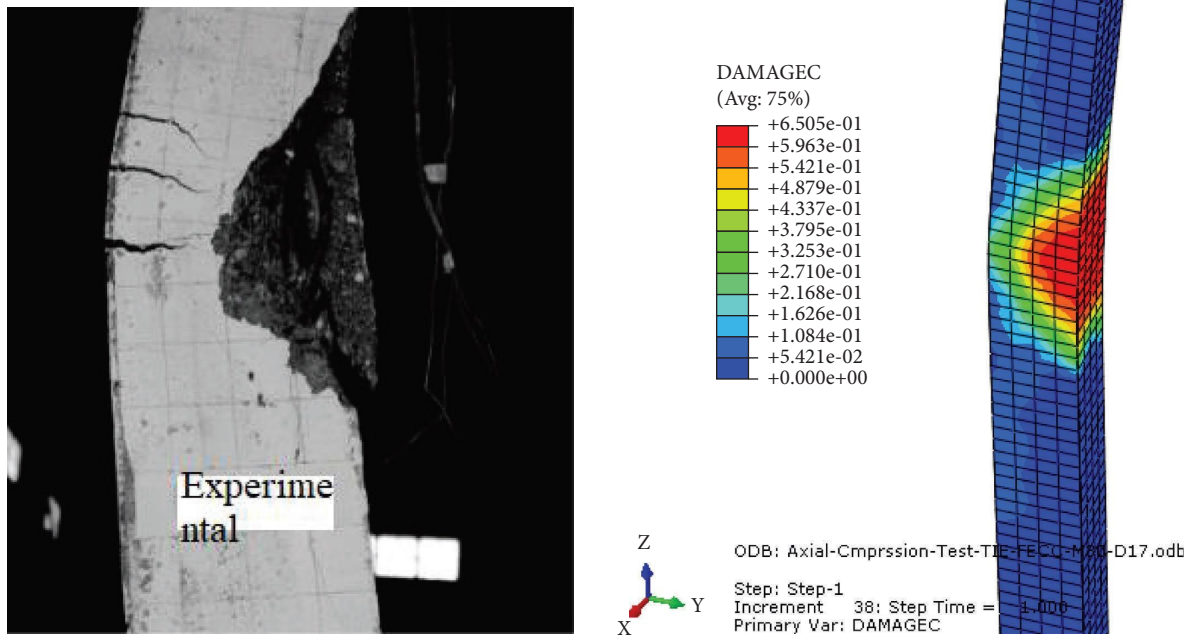
FIGURE 5: Concrete spalling and tensile cracking of experimental and numerical column of [4].
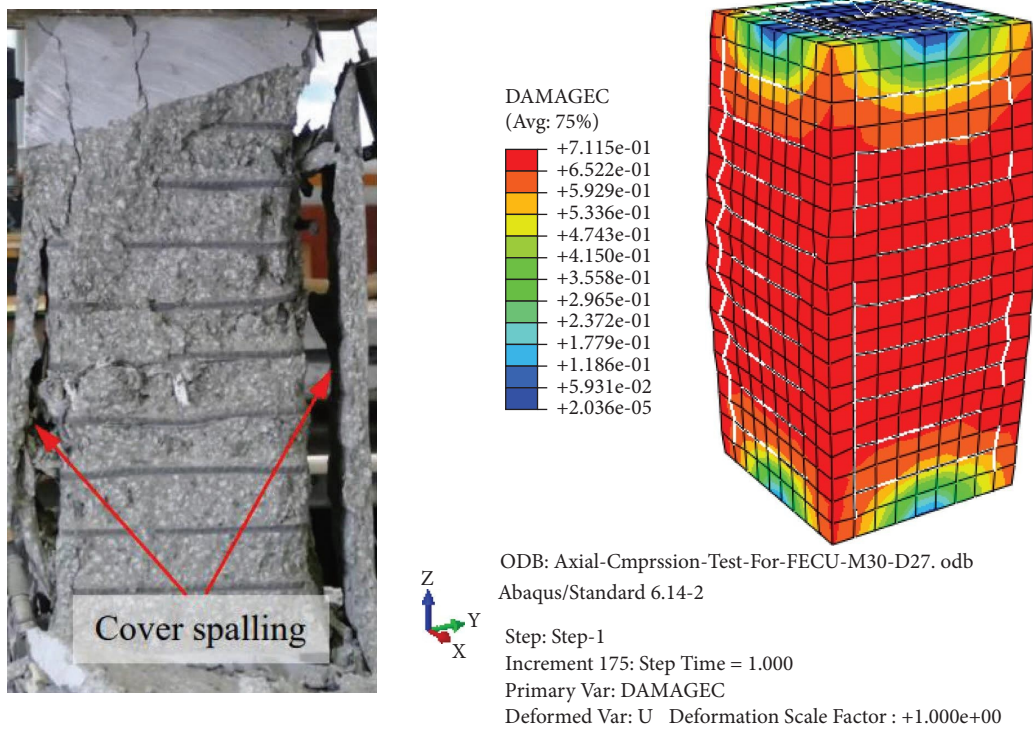

FIGURE 6: Concrete cover spalling of experimental and numerical column of [6].

elastic materials up until the point of yielding, beyond which they exhibit nonlinear plastic behavior. As presented in Table 1, this study employs the linear strain-hardeningelastic-plastic model [16, 17]. Elasticity and plasticity parameters are present in this model. The plasticity model is used to define the nonlinear linear plastic behavior of these materials, while the elastic option is used to define the linear elastic material behavior. Young's modulus of elasticity of 210 GPa is used for both structural steel and 200 GPa is used for main bars and tie bars. Poisson's ratio of 0.3 is used for all.

The typical true stress-plastic strain curve of the current study was considered for modeling. The material and the

Axial Load vs Axial Deformation

RHC1S3   ISHC1S3
CSHC1S3   RSHC1S3

(a)

Axial Load vs Axial Deformation

RHC1S1   ISHC1S1
CSHC1S1   RSHC1S1

(b)

Axial Load vs Axial Deformation

RHC2S3   ISHC2S3
CSHC2S3   RSHC2S3

(c)

Axial Load vs Axial Deformation
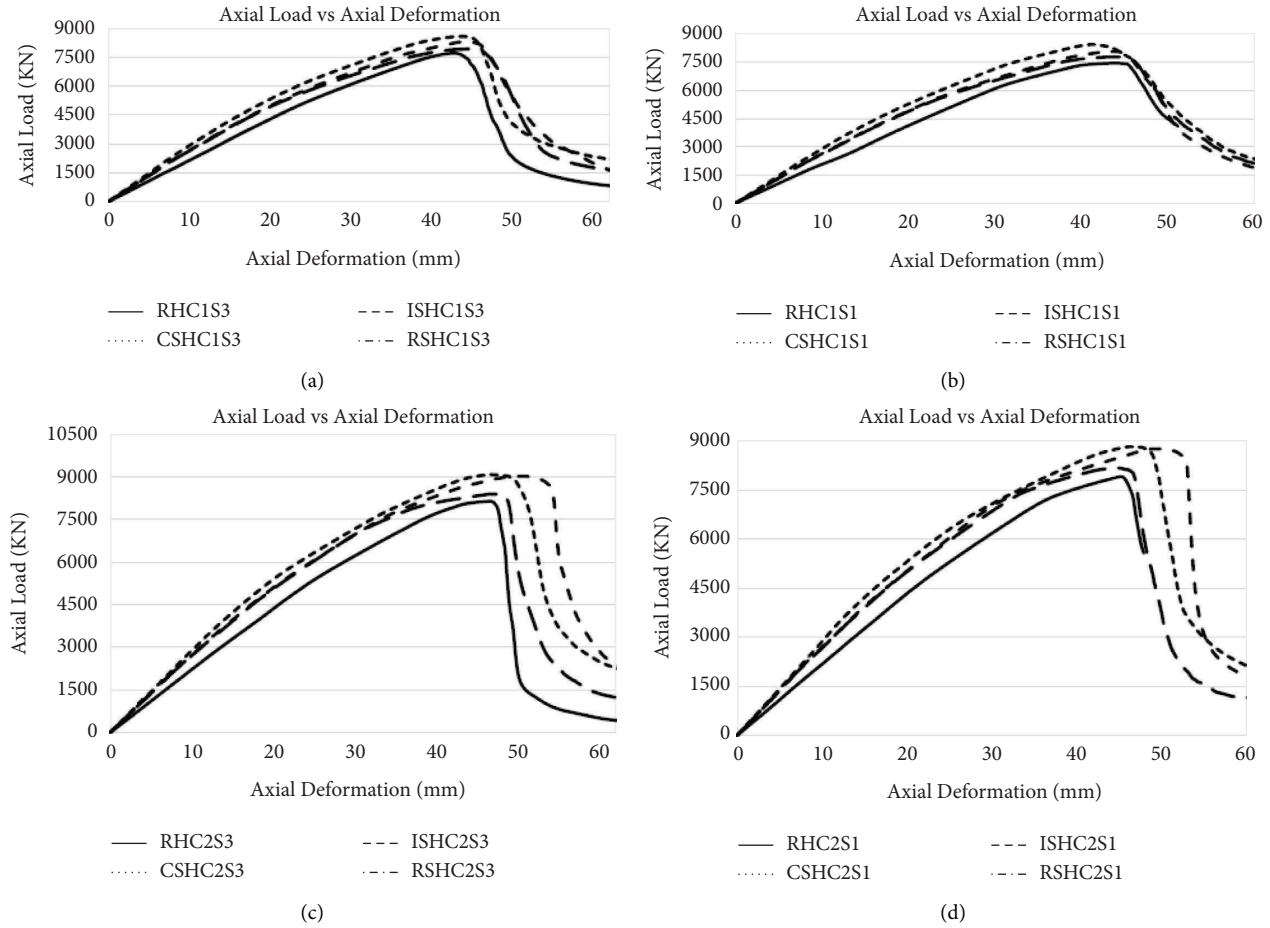
RHC2S1   ISHC2S1
CSHC2S1   RSHC2S1

(d)

Figure 7: Effect of HSC on axial load-axial deformation response of (a) RC slender columns and FEC slender columns with (b) circular, (c) I-shaped, and (d) rectangular steel encasement.

behavior of structural steel sections and reinforcements are shown in Figure 1.

2.3.2. Concrete Modeling.

Since ES EN 1994: 2013 only addresses the design of composite structures with concrete grades between C-20/25 and C-60/75, modeling of high-strength concrete should be performed with reference to [18]. In this thesis, concrete with f_{ck} of up to 60 MPa is referred to as "normal-strength concrete" (NSC), while concrete with f_{ck} of between 60 MPa and 120 MPa is referred to as "high-strength concrete" (HSC). The term "ultrahigh-strength concrete" is used when the concrete's f_{ck} strength is greater than 120 MPa (UHSC). The current study focuses on HSC because the majority of earlier studies only examined concrete compressive strength up to C90/105 (as summarized in Table 2).

The mechanical properties of concrete are almost always related to the tangent mean value of compressive strength f_{cm} but not the characteristic strength f_{ck}. Therefore, f_{cm} is calculated as

$$f_{cm} = f_{ck} + \Delta f, \tag{1}$$

where $\Delta f = 8 MPa$ stands for cylinder and $\Delta f = 10 MPa$ stands for cube.

When no test results are available to determine the stress-strain curve for the concrete, one can use the actual tangent mean value of the compressive strength of concrete, f_{cm}, to plot the curve. Then, modulus of elasticity, E_{cm}, can be estimated from the following equation using article [3]. Poisson's ratio of concrete (μ_c) is considered to be a constant ranging from 0.14 to 0.26 based on tests by different researchers in [19]. In this study, it is assumed to be 0.2 for all concrete grades.

$$E_{cm} = 22 * (0.1 * f_{cm})^{0.3}. \tag{2}$$

The typical stress-strain curves used in the current FE model for unconfined and confined concrete with the mean compressive strength (f_{cm}) ranging from 98 to 128 MPa are shown in Figure 2.

TABLE 10: Effect of concrete compressive strength on the peak load capacity of slender columns.

Column type	Column ID	Peak axial load (N_{num})	Percent difference (%)	Column type	Column ID	Peak axial load (N_{num})	Percent difference (%)
Control RCC	RCH1S1	7442.67	—	FECC-I	ISHC1S1	8074.95	—
	RCH2S1	7896.18	6.09		ISHC2S1	8745.25	8.3
	RCH3S1	8896.69	19.54		ISHC3S1	9800.41	21.37
FECC-C	CSHC1S1	8320.52	—		RSHC1S1	7649.10	—
	CSHC2S1	8799.52	5.76		RSHC1S1	8165.45	6.75
	CSHC3S1	9898.05	18.96		RSHC1S1	9108.08	19.07

TABLE 11: Effect of structural steel shape on the axial load capacity of FEC column with $s = 50$ mm.

Group	Column ID	Structural steel	Concrete f_{ck}, (MPa)	S (mm)	Peak axial load (P)	Percent difference (%)
Group 1	Control RHC1	—	90		7734.38	—
	HC1CS	Circular	90	50	8620.64	11.46
	HC1IS	I-shaped	90		8315.56	7.51
	HC1RS	Rectangular	90		7956.81	2.88
Group 2	Control RHC2	—	100		8148.87	—
	HC2CS	Circular	100	50	9086.14	11.50
	HC2IS	I-shaped	100		9024.55	10.75
	HC2RS	Rectangular	100		8406.18	3.16
Group 3	Control RHC3	—	120		9164.90	—
	HC3CS	Circular	120	50	10104.70	10.25
	HC3IS	I-shaped	120		9998.76	9.10
	HC3RS	Rectangular	120		9495.37	3.61

2.4. Parametric Study.

To evaluate the impact of various parameters on the strength and responsiveness of the columns, parametric research is carried out using the model on 36 (thirty-six) FEC thin columns. Tables 3 and 4, respectively, list the geometrical and material characteristics of the column specimens for reinforcements, structural steel, and concrete that were employed in the finite element study. Figure 3 displays the cross-sections and 3D views of typical FEC columns.

2.4.1. Geometrical Properties of Column Specimens.

Each rectangular FEC thin column has a cross-section of 300 mm by 250 mm and a length of 9000 mm. Concrete, structural steel (circular, I-shaped, and rectangular) encasements, and reinforcing bars (12 mm main bar and 8 mm tie bar) are used to build these columns. They are numerically simulated for axial loading conditions that are concentric.

The word "Circ" in Table 3 stands for circular steel pipe whereas "Rect' stands for rectangular steel pipe. Where $(h \times b_f \times t_w \times t_f)/(D \times t)$ (mm) in the table are the overall dimensions of the structural steel sections with b_f being the flange width, h being the total depth, t_w being web thickness, and t_f being the flange thickness of rectangular steel tube and I-shaped steel section while D and t are the diameter and thickness, respectively, of the circular steel tube section which are shown in Figures 3(a) and 3(b).

2.4.2. Material Properties of Column Specimens.

The compressive strengths of concrete used in the current study are 90 MPa, 100 MPa, and 120 MPa. The yield strengths (f_y) and ultimate strengths (f_u) of structural steel, main bar, and tie bar are $F_{ya} = 355$ MPa and $F_{ua} = 457.95$ MPa; $F_{ys} = 460$ MPa and $F_{us} = 541.65$ MPa; and $F_{ys} = 500$ MPa and $F_{us} = 581.25$ MPa, respectively, from [6, 14] as shown in Table 4.

2.4.3. Parameter Variations.

The effects of various parameters influencing the behavior of FEC slim columns are evaluated in this parametric study. The crucial variables are the tie bar spacing, various shapes of structural steel encasements, and compressive strength of concrete (f_{ck}). For the final discussion and result interpretation, the variables were switched during the FE analysis. It should be noticed that one parameter is altered while leaving the remaining parameters fixed when performing the FE analysis of FEC thin columns. The parameters that will be looked at determine which columns will be used. The next sections provide detailed descriptions of the effects of column specimen parameter changes.

(1) Investigating the Effects of Compressive Strength of Concrete (f_{ck}). A total of twelve samples of columns (three RC and nine FEC slender columns) are developed to investigate the effects of three different compressive characteristic cylindrical strengths of concrete (90 MPa, 100 MPa, and 120 MPa) on the behavior of the columns. The yield strength of structural steel is 355 MPa. The spacing of tie bars is 100 mm for all columns. Detailed descriptions of the specimens are shown in Table 5.

(2) Investigating the Effects of Structural Steel Encasements. Twenty-four column specimens (six control-RC and eighteen FEC columns) made with HSC (90 MPa, 100 MPa, and 120 MPa) are developed to assess the effects of three different types of fully encased steel sections (circular, I-shaped, and rectangular encasements). The yield strength of structural steel is 355 MPa. The spacing of tie bars is 50 mm and 100 mm. Detailed descriptions of the specimens are shown in Table 6.

(3) Investigating the Effects of Tie Bar Spacing (s). Here, a total of twenty-seven FEC slender column specimens are taken to study the effects of spacing of tie bars (50 mm, 100 mm, and 150 mm). The columns are made with three different compressive strengths of concrete (90 MPa, 100 MPa, and 120 MPa) and three different types of fully encased steel sections (circular, I-shaped, and rectangular). The yield strength of structural steel is 355 MPa for all columns. Detailed descriptions of the specimens are outlined in Table 7.

2.5. Validation of the Finite Element Model.

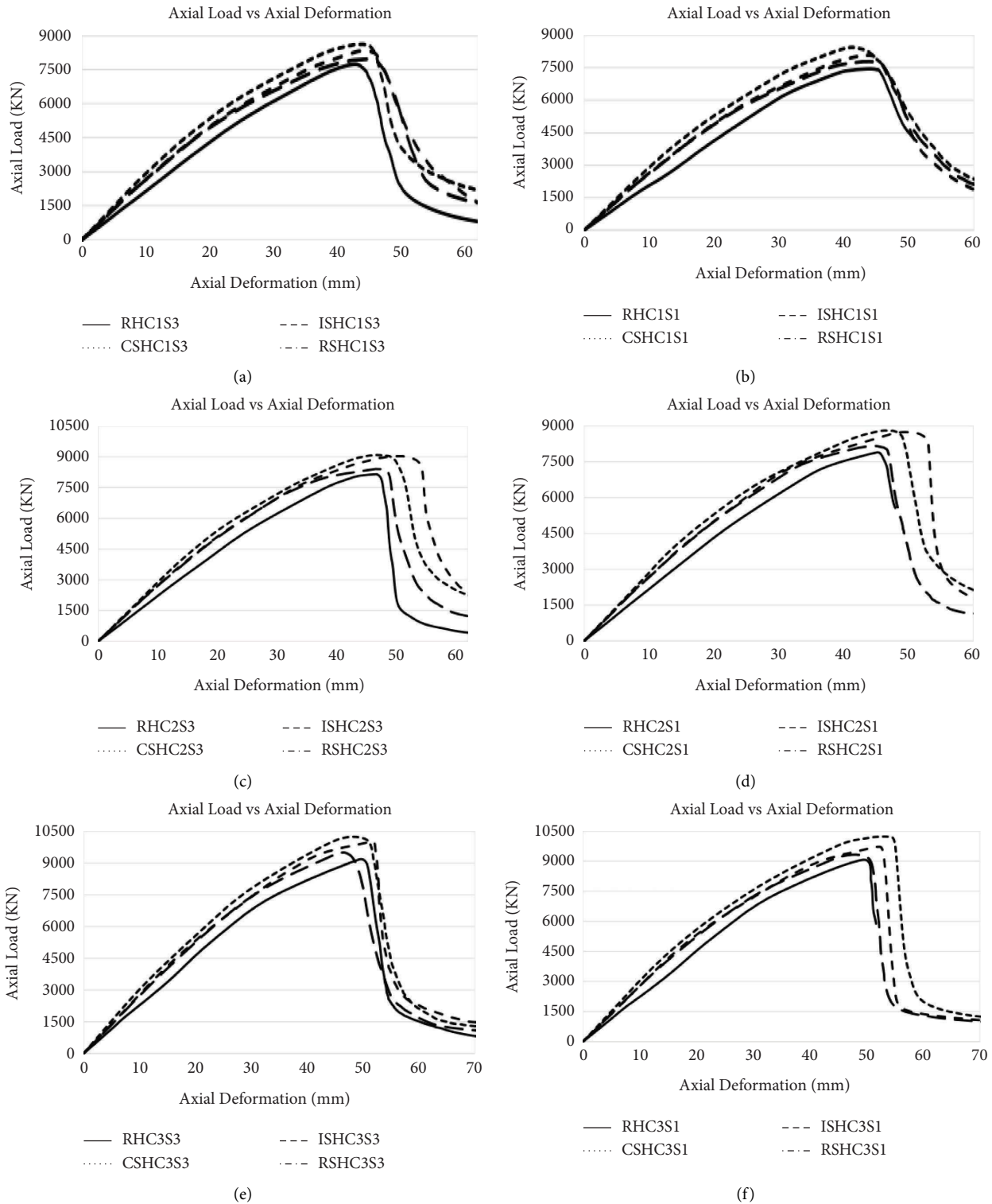The numerical outcomes of ABAQUS 6.14-2 finite element analysis are

FIGURE 8: Effect of structural steel shape on load-deformation response: (a) group 1, $s = 50$ mm; (b) group 1, $s = 100$ mm, (c) group 2, $s = 50$ mm, (d) group 2, $s = 100$ mm, (e) group 3, $s = 50$ mm, and (f) group 3, $s = 100$ mm.

validated in comparison to earlier concentric load experimental data. To confirm the finite element modeling of FEC columns created using NSC and HSC, the four experimental test specimens "A1" created by [4], "C7 and C9" created by [14], and "S690-C90-SP60-H" created by [6] were selected.

The geometrical properties and material properties of the selected FEC test columns for validation are shown in Tables 8 and 9, respectively.

The comparisons are made between the results of finite element analysis and experimental studies in terms of axial

TABLE 12: Effect of structural steel shape on the axial load capacity of FEC column with $s = 100$ mm.

| Group	Column ID	Structural steel	Concrete f_{ck}, (MPa)	S (mm)	Peak axial load (P)	Percent difference (%)
Group 1	Control RHC1	—	90	100	7442.67	—
	HC1CS	Circular	90		8320.52	11.79
	HC1IS	I-shaped	90		88074.95	8.50
	HC1RS	Rectangular	90		7649.10	2.77
Group 2	Control RHC2	—	100	100	7996.18	—
	HC2CS	Circular	100		8799.52	11.44
	HC2IS	I-shaped	100		8745.25	10.75
	HC2RS	Rectangular	100		8165.45	3.41
Group 3	Control RHC3	—	120	100	8896.69	—
	HC3CS	Circular	120		9898.05	10.12
	HC3IS	I-shaped	120		9800.41	9.22
	HC3RS	Rectangular	120		9108.08	2.32
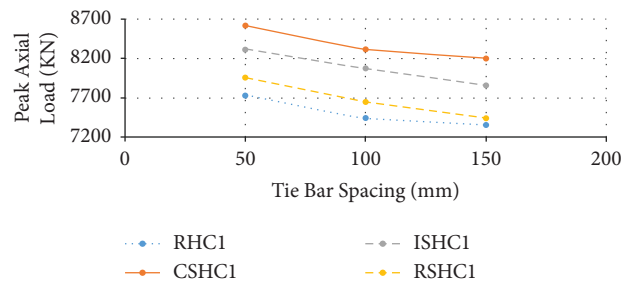
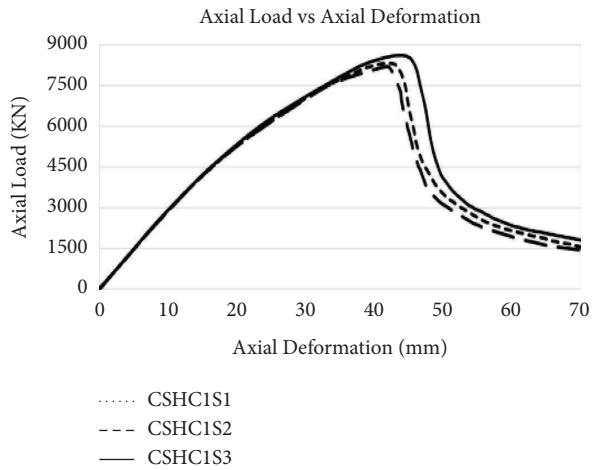FIGURE 9: Effect of tie bar spacing on peak axial load of RCC and FECC with 90 MPa HSC.

load versus axial deformation response, peak axial load and peak axial strain, modes of failure, and damage pattern. Figures 4(a)–4(d) show the comparisons between the experimental and numerical axial load versus axial deformation curves for the four verified FEC column specimens. The failure mode of the column specimens A1 and S690-C90-SP60-H from the experiment and finite element analysis is shown in Figures 5 and 6.

As plotted in Figures 4(a)–4(d), the numerical results overestimate the peak axial load by 6.14%, 2.07%, 2.56%, and 15.95% for FEC columns A1, C7, C9, and S690-C90-SP60, respectively. The ratios of numerical results to experimental results are between 1.021 and 1.19. This indicates that the FE models are capable of predicting the peak axial load versus deformation of the investigated FEC columns made with high-strength concrete. It is observed that good agreement between the experiment and the numerical results has been attained. Therefore, the developed FE models can be used in the parametric study to investigate the various parameters affecting the performance of FEC columns. The failure modes of the columns are spalling of concrete cover and crushing of concrete in the compression side. In addition, buckling of longitudinal rebar and crushing of the confined concrete are noticed in the experimental specimen. It is seen that the failure mode and damage pattern identified from the numerical results are similar to the experiment results, as shown in Figures 5 and 6.
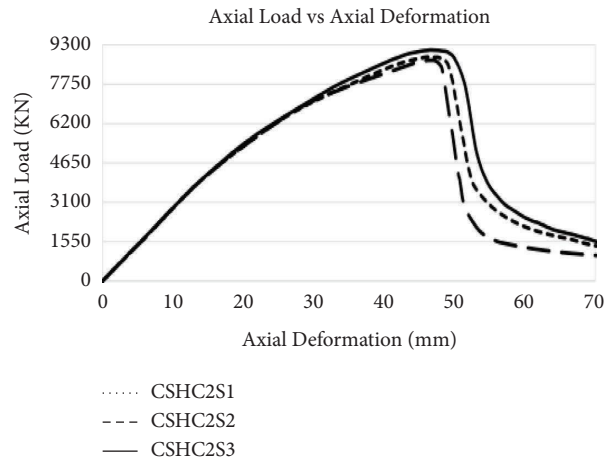
3. Results and Discussion

3.1. Results and Discussion of the Effect of Selected Parameters on Column Response.
In this study, the condition of stresses is analyzed using the damage plasticity analysis method for concrete and the elastic-plastic analysis method for steel sections and rebar. These techniques allow for the ignoring of the minor force along the steel thickness. As a result, the plane-stress condition is taken into account, and the steel sections and rebar's yielding behavior are described using the von Misses yield criterion. To investigate the impact of various parameters on the response of RC and FEC slender columns under concentric axial loads, a total of 36 slender column specimens are numerically simulated. Axis load versus axial deformation curve, peak axial load and the corresponding axial deformation at the peak load, ductility index, and the failure modes of the columns such as concrete compression damage, concrete tension damage, and von Misses stresses are the output parameters extracted from the finite element analysis results. The following subsections present the effects of each parameter and a discussion of the findings.
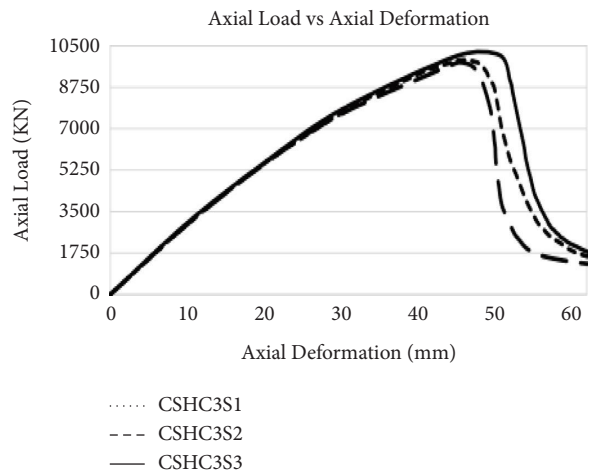
3.1.1. Effect of Compressive Strength of Concrete.
To evaluate the impact of concrete compressive strength on the behavior of the columns, three samples of RC slender columns and nine samples of FEC slender columns produced with three different types of steel sections and 100 mm spacing of tie bars are taken into consideration (see Table 5). Concrete has
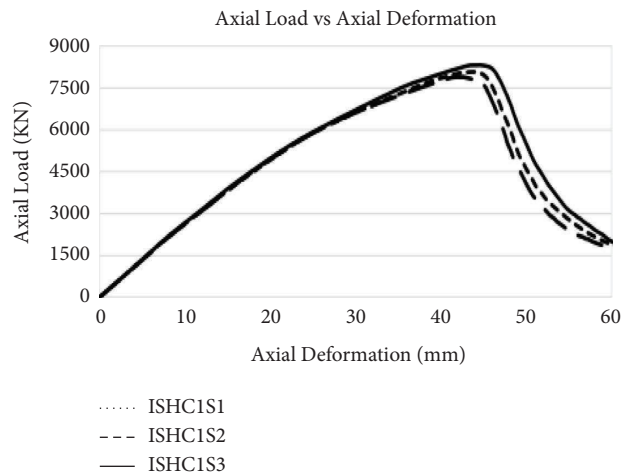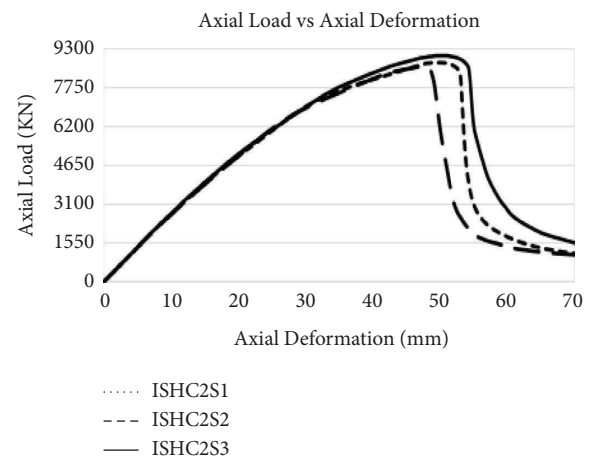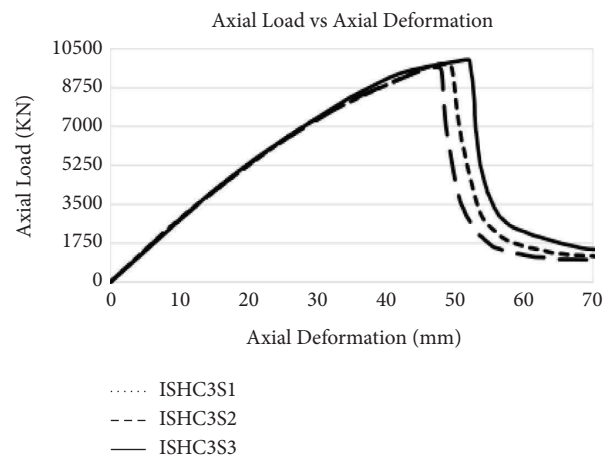
Axial Load vs Axial Deformation

...... CSHC1S1
--- CSHC1S2
— CSHC1S3

(a)

...... CSHC2S1
--- CSHC2S2
— CSHC2S3

(b)

...... CSHC3S1
--- CSHC3S2
— CSHC3S3

(c)

...... ISHC1S1
--- ISHC1S2
— ISHC1S3

(d)

...... ISHC2S1
--- ISHC2S2
— ISHC2S3

(e)

...... ISHC3S1
--- ISHC3S2
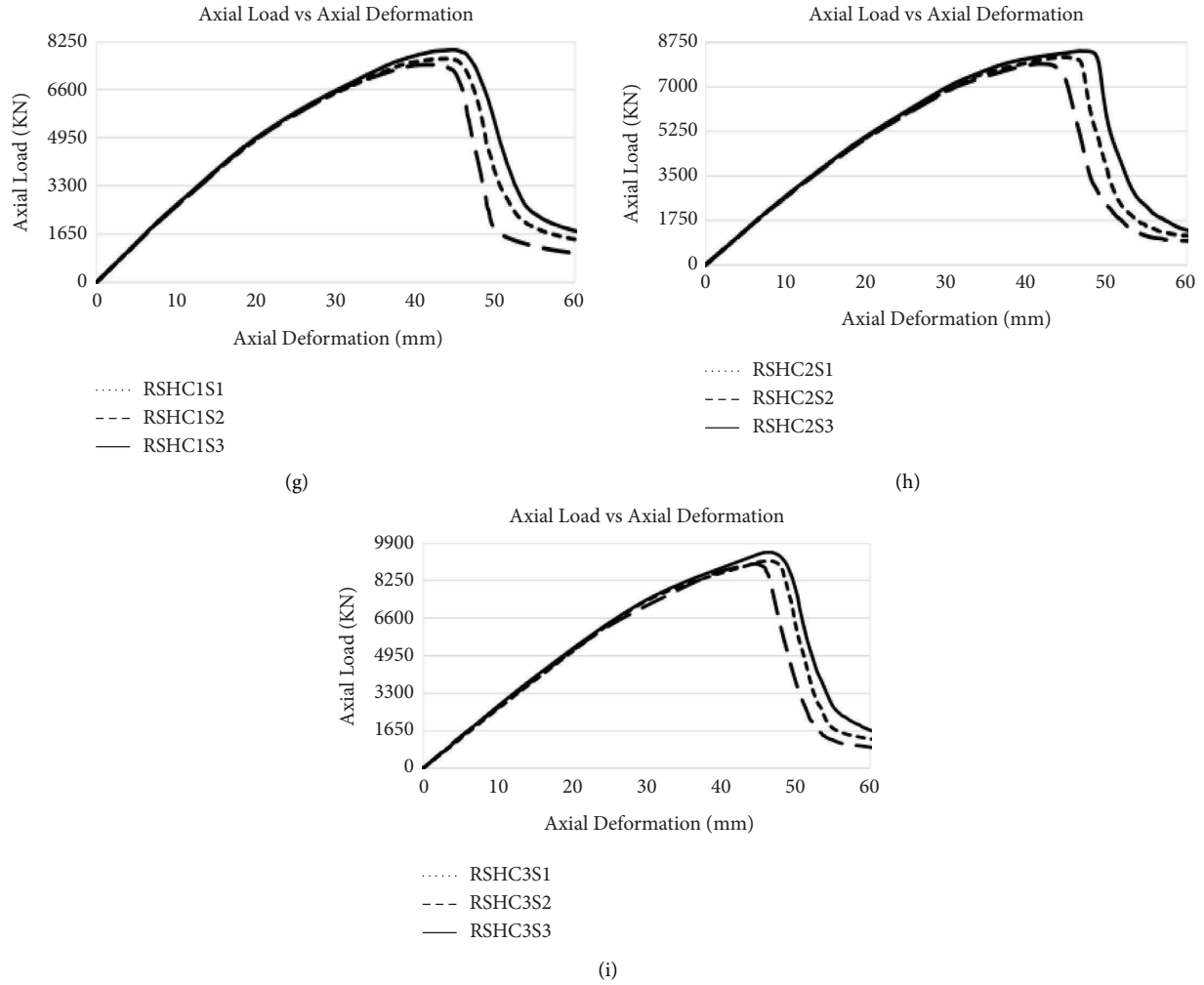— ISHC3S3

(f)

Figure 10: Continued.

(g)

(h)

(i)

FIGURE 10: Effect of tie bar spacing on axial load versus axial deformation response of FECC-C (a–c), FECC-I (d–f), and FECC-R (g–i) slender columns.

TABLE 13: Ductility index of columns due to structural steel shapes.

Column ID	Structural steel sections	Concrete F_{ck} (MPa)	S (mm)	Peak axial load (P)	Axial deformation		Ductility index ($\mu = \Delta_{0.75p}/\Delta p$)
					Δ	$\Delta_{0.75p}$	
Control-RCH1	—	90		7734.38	42.69	46.44	1.09
HC1CS	Circular	90		8620.64	43.99	51.08	1.16
HC1IS	I-shaped	90	50	8315.56	44.07	50.24	1.14
HC1RS	Rectangular	90		7956.81	45.00	51.40	1.14
Control-RCH2	—	100		7896.18	45.14	47.58	1.05
HC2C2	Circular	100		8799.52	47.64	53.36	1.12
HC2IS	I-shaped	100	100	8745.25	49.64	53.45	1.08
HC2RS	Rectangular	100		8165.45	44.82	49.30	1.10
Control-RCH3	—	120		8791.67	46.08	47.10	1.02
HC3CS	Circular	120		9782.54	45.94	49.68	1.08
HC3IS	I-shaped	120	150	9647.87	46.60	48.61	1.04
HC3RS	Rectangular	120		8973.71	44.83	47.65	1.06

TABLE 14: Ductility index of columns due to spacing of tie bars.

| Column type	Column ID	Concrete F_{ck} (MPa)	S (mm)	Peak axial load (P)	Axial deformation		Ductility index ($\mu = \Delta_{0.75p}/\Delta p$)
					Δ	$\Delta_{0.75p}$	
RCC	RHC1s1		100	7442.67	43.35	46.38	1.07
	RHC1s2	90	150	7350.93	23.52	24.77	1.05
	RHC1s3		50	7734.38	42.69	46.44	1.09
FECC-C	CSHC1s1		100	8320.52	42.34	47.48	1.12
	CSHC1s2	90	150	8201.11	41.55	46.17	1.11
	CSHC1s3		50	8620.64	43.99	51.08	1.16
FECC-I	ISHC1s1		100	8074.95	43.74	48.12	1.10
	ISHC1s2	90	150	7853.53	41.02	44.72	1.09
	ISHC1s3		50	8315.56	44.07	50.24	1.14
FECC-R	RSHC1s1		100	7649.10	43.49	48.28	1.11
	RSHC1s2	90	150	7441.27	40.35	44.39	1.10
	RSHC1s3		50	7956.81	45.00	51.40	1.14
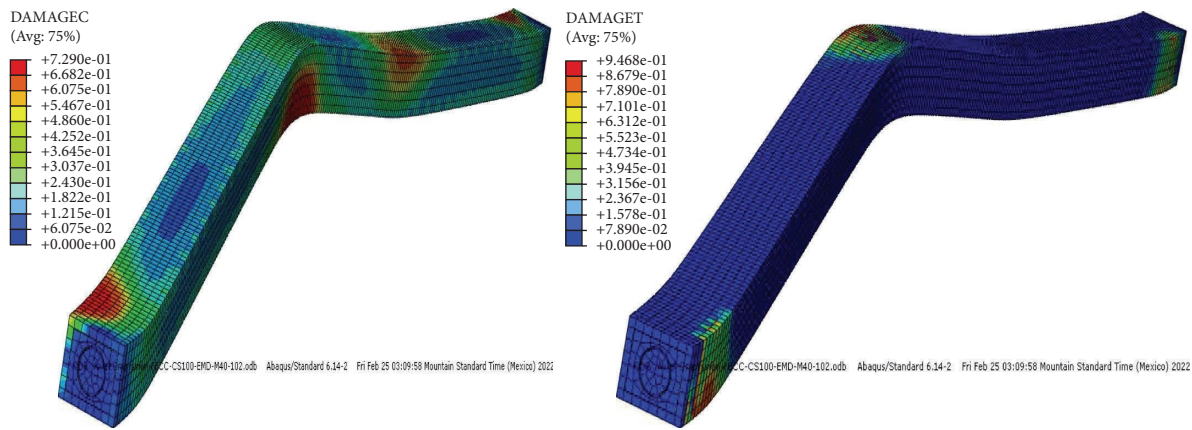
FIGURE 11: Stress components and crack pattern of concrete in compression and tension.

strengths ranging from 90 MPa, 100 MPa, and 120 MPa. The steel used for construction has a 355 MPa yield strength.

(1) Axial Load versus Axial Deformation Behavior. Figures 7(a)–7(d) illustrate the impact of three different concrete compressive strengths on the axial load versus axial deformation behavior (D). The findings show that the strength of concrete has a considerable impact on the load-carrying capability of the RC and FEC slender columns. Table 8 shows how HSC (90 MPa, 100 MPa, and 120 MPa) affects load-carrying capacity. Concrete strength increments are computed from 90 MPa to 100 MPa and from 100 MPa to 120 MPa.

From Table 10, when compared to the peak axial load capacity of the RHC1S1 column, the peak axial load capacities of the RHC2S1 and RHC3S1 columns are enhanced by 6.09% and 19.54%, respectively. However, as compared to the peak axial load capacity of the CSHC1S1 column, the peak axial load capacities of the CSHC2S1 and CSHC3S1 columns have increased by 5.76% and 18.96%, respectively. The peak axial load capacities of the ISHC2S1 and ISHC3S1 columns are also higher than those of the ISHC1S1 column, increasing by 8.30% and 21.37%, respectively. Additionally,

as compared to the peak axial load capacity of the RSHC1S1 column, the peak axial load capacities of the RSHC2S1 and RSHC3S1 columns have grown by 6.75% and 19.07%, respectively. However, as concrete strength is increased, the columns' ductility is reduced. As a result, immediately following the peak load, a sharp decline in the axial load versus axial deformation curves is observed.

3.1.2. Effect of Structural Steel Shapes. As illustrated in Table 11, twenty-four columns divided into three groups are used to examine the impact of structural steel shape. These three groupings are separated according to the various concrete strengths (90 MPa, 100 MPa, and 120 MPa). The 90 MPa high-strength concrete used to replicate the columns in group 1 was used to model columns RHC1, HC1CS, HC1IS, and HC1RS. Columns control-RHC2, HC2CS, HC2IS, and HC2RS were composed of Group 2. The concrete used to simulate these columns has a strength of 100 MPa. Similar to Group 2, Group 3 used high-strength concrete (120 MPa) to replicate the columns control-RHC3, HC3CS, HC3IS, and HC3RS. Tie bars are spaced 50 mm and 100 mm apart. Numerical simulations are performed for each group of FEC thin columns using three distinct
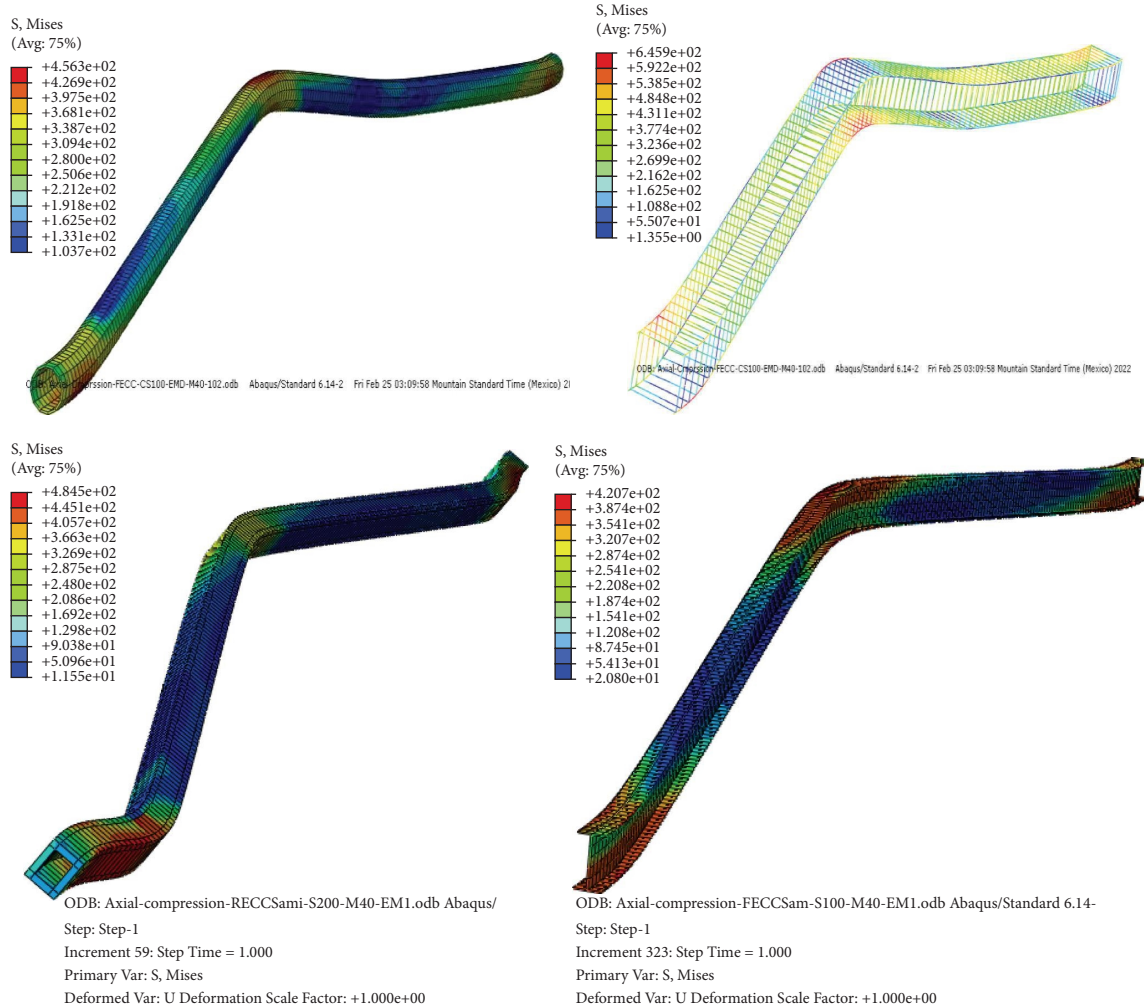
FIGURE 12: Deformed shape with stress contour of structural steel and rebar at failure.

structural steel shapes (circular, I-shaped, and rectangular). The next sections present their influence on the general behavior and load-carrying capability of FEC columns.

3.1.3. Axial Load versus Axial Deformation Behavior. Figures 8(a)–8(f) show the axial load versus axial deformation behavior for Group 1, 2, and 3 columns with different structural steel forms. The results show that the presence of various structural steel shapes increases the stiffness and load-carrying capacity of control-RC thin columns. The columns' ductility has also been greatly improved. Within the three groups of columns with a stirrup spacing of 50 mm and 100 mm, this behavior is seen.

Figures 8(a)–8(f) revealed that columns in Groups 1, 2, and 3 showed an improvement in axial load capacity when structural steel shapes are used. All columns exhibited the same behavior. To further quantify the effect of structural steel shapes, enhancement in numerically obtained axial capacities of the columns within each group are reported in Tables 11 and 12. The increments of numerical loads in

percent are determined with respect to the control-RC slender columns within each group.

It is seen from Tables 11 and 12 that the axial load capacity of columns HC1RS, HC1IS, and HC1CS in group 1 is observed to be 2.8%, 7.5%, and 11.5% which is higher than that of the control-RHC1. Similarly, the load capacities of columns HC2RS, HC2IS, and HC2CS in group 2 are enhanced by 3.2%, 10.8%, and 11.4%, respectively, than column control-RHC2. Likewise, for columns in group 3, the load capacity of columns is improved by 2.3%, 9.1%, and 10.1%, respectively. Moreover, as it is obviously expected, a higher load capacity is observed in FEC slender columns made with circular steel tubes encased in concrete than in other columns.

3.1.4. Effect of Tie Bar Spacing. Tie bar spacing has a significant impact on the ductility, confinement, and early crushing of concrete while building columns. To see how tie bar spacing affects column response, 27 FEC thin columns are numerically simulated. In this investigation, three

different tie bar spacing are used, namely, 50 mm, 100 mm, and 150 mm. Figure 9 plots the peak axial load versus tie bar spacing for the twelve samples of 90 MPa HSC columns so that the effect is clearly seen.

As seen from Figure 9, the axial load capacity of the columns is slightly increased by reducing the spacing of tie bars. Hence, the adoption of closely spaced tie bars improves the load-carrying capacity of FEC slender columns with HSC under concentric axial loads.

(1) Axial Load versus Axial Deformation Behavior. Figure 10 shows the axial load versus axial deformation behavior for the FEC columns under investigation (A-I). Since all of the columns had comparable behavior, it can be seen from the figures that reducing the tie bar spacing had no effect on their ascending branches though the variable tie bar spacing affects the columns' descending branch (post-peak behavior).

3.1.5. Ductility Index for Columns. The ductility index (μ) is the ratio of the deformation at peak load (Δp) and postpeak deformation ($\Delta 0.75p$) corresponding to 75% of the peak load. Table 13 shows that the FEC columns made with HSC (90 MPa and 100 MPa) behave in a relatively ductile manner. On the other hand, a sudden drop in the axial load-axial deformation curves is observed right after the peak load of FEC columns made with 120 MPa of HSC as shown in Table 14. This is because of the fact that the concrete strength increases the ductility of the column reduces. This phenomenon is more experienced in FECC-I. However, the FECC-C is relatively more ductile. Hence, for FEC slender columns with HSC greater than 100 MPa, tubular steel encasements are preferable in both ductility and residual strength after failure. The ductility index due to the spacing of tie bars is reported in Table 14. The table shows that the FEC slender columns made with 50 mm spacing of tie bars are relatively more ductile. Therefore, it is concluded that the adoption of closely spaced tie bars in the construction of FEC columns resulted in good ductility.

3.1.6. Modes of Failure of the Columns. Near the peak load of the columns, the axial load versus axial deformation curves gradually changed from linear to bending. This shows that the concrete has begun to crack and the stirrups have begun to enclose. These surface cracks on the columns are always an indication that the column has reached its failure stage. The current study's RC and FEC columns both fail in essentially the same way. The results of the finite element study revealed that the structural steel and rebar of the FEC stub columns underwent rapid transverse elongation due to dilatation (bulging) of the concrete, which caused the columns to shorten longitudinally. These induce transverse tension and cause yielding of the steel section and rebar. As compression grew past the peak load, the columns could collapse due to concrete crushing and structural steel and rebar yielding. For the FEC slender columns, however, the longitudinal bar and structural steel reached their yield stress at the compression and tension

sides, and concrete damage (concrete crushing on the compression side and tensile cracks on the opposite side) also happened in the region where the severe column buckling was located as well as in the upper or lower part of the column. As a result, the components' strength is not properly used. The FEC slim columns exhibit a failure mechanism that is defined by a worldwide buckling (instability) failure with a critical section at or near the midheight or 1/4-height of the columns, where it may be deduced. Figures 11 and 12 show the FEC slim column failure modes that were seen in the FEA. Figure 11 depicts the stresses and concrete failure fracture pattern. At or near the midheight of FEC thin columns, the von Mises stress on the steel section and rebar is found to yield and all tie bars do not reach their yield strength at the tension side of all columns.

4. Conclusions

This study uses the finite element code ABAQUS [20] to conduct a numerical simulation in order to examine the behavior of FEC thin columns with HSC under concentric axial load. The following results were reached after a total of 36 columns were numerically studied and the effects of various parameters, including the compressive strength of concrete, structural steel forms, and tie bar spacing, were evaluated.

(i) The higher compressive strength of concrete resulted in the higher load-carrying capacity of fully encased composite slender columns.

(ii) Behavior of concrete was obviously influenced due to the presence of encased structural steel shapes. FECC-I with HSC of 120 MPa showed more brittle failure but FECC-C showed good confinement and resulted in enhanced load capacity and ductility.

(iii) Significant enhancements in the axial load capacity were observed in the case of FEC slender columns significant to RC slender columns of the same size and shape.

(iv) Ductility and residual strength after the failure of FEC columns were also observed to increase significantly with the adoption of tubular structural steel sections. However, increasing the concrete strength resulted in a reduction of this ductility.

(v) The axial load capacity of the columns was slightly increased by reducing the spacing of tie bars. Hence, the adoption of closely spaced tie bars improved the load-carrying capacity of FEC slender columns with HSC under concentric axial loads.

Nomenclature

CFST: Concrete-filled steel tubes
CES: Concrete-encased steel
FE: Finite element
FEC: Fully encased composite
FEA: Finite element analysis

HSC: High-strength concrete
C3D4: A continuum 3-dimensional 4-node linear tetrahedron
HSM: High-strength materials
RCC: Reinforced concrete column
DOFs: Degrees of freedoms
NSC: Normal strength concrete
PEC: Partially encased composite
FECC-C: Fully encased composite column with circular steel tube encasements
FECC-I: Fully encased composite column with I-shaped steel encasements
FECC-R: Fully encased composite column with rectangular steel tube encasements.

Data Availability

The data used to support the findings of the study can be obtained from the corresponding author upon request.

Conflicts of Interest

The authors declare that they have no conflicts of interest..

Authors' Contributions

All authors contributed to the study's conception and design. Material preparation, data collection, and analysis were performed by Getinet Melsse, Samuel Jima, Tegegn Asale, Hibretu Kaske Kassa, and Yayesew Moges. The first draft of the manuscript was written by Hibretu Kaske Kassa and all authors commented on previous versions of the manuscript. All authors read and approved the final manuscript. All authors were actively involved in reviewing and correcting the given comment by reviewers.

Acknowledgments

References

[1] T. A. Kartheek, "3D modelling and analysis of encased steel-concrete composite column using ABAQUS," *Materials Today Proceedings*, vol. 27, pp. 1545–1554, 2020.

[2] M. A. Khan, "Parametric study on high strength ECC-CES composite columns under axial compression," *Journal of Building Engineering*, vol. 44, 2021.

[3] Ebcs En 1994-1-1, 2013, "Design of composite steel and concrete sructures," in *General Rules and Rules for Buildings*, Ethiopian Building Construction, Addis Ababa, Ethiopia, 2013.

[4] M. L. J. Zhu, "Experimental research on square steel tubular columns filled with steel-reinforcedself-consolidatinghigh-strength concrete under axial load," *Engineering Structures*, vol. 32, no. 8, pp. 2278–2286, 2010.

[5] M. Rahman, *Behavior and Strength of Fully Encased Composite Columns*, Bangladesh University of Engineering And Technology, Dhaka, Bangladesh, 2016.

[6] B. L. Lai, "Assessment of high-strength concrete encased steel composite columns subject to axial compression," *Journal of Constructional Steel Research*, vol. 164, 2020.

[7] M. A. Mansur, "Considerations in producing high strength concrete," *Journal of Civil Engineering*, vol. 37, no. 1, pp. 53–63, 2009.

[8] H. K. Kassa, "A study on using glass fiber-reinforced polymer composites for shear and flexural enhancement of reinforced concrete beams," *Advances in Civil Engineering*, vol. 2022, Article ID 5995103, 12 pages, 2022.

[9] W. A. Anuntasena, "Finite element modelling of concrete-encased steel columns subjected to eccentric loadings," *Engineering Journal*, vol. 23, no. 6, pp. 299–310, 2019.

[10] F. A. Li, "Axial behavior of reinforced PP-ECC column and hybrid NSC-ECC column under compression," *Engineering Structures*, vol. 195, pp. 223–230, 2019.

[11] X. A. Wang, "Bond strength prediction of concrete-encased steel structures using hybrid machine learning method," *Structures*, vol. 32, pp. 2279–2292, 2021.

[12] B. a. Lai, "Buckling behaviour of high strength concrete encased steel composite columns," *Journal of Constructional Steel Research*, vol. 154, pp. 27–42, 2019.

[13] Abaqus Analysis User Manual, *Abaqus Version 6.8*, Abaqus Analysis User Manual, Rising Sun Mills, USA, 2008.

[14] K. Z. Soliman, "Review of design codes of concrete encased steel short columns under axial compression," *Journal House and Building National Research Center (HBRC), Cairo, Egypt*, vol. 19, no. 2, pp. 134–143, 2013.

[15] N. A. Hong, "Part I: the analytical model predicting post-yield behavior of concrete-encased steel beams considering various confinement effects by transverse reinforcements and steels," *Journal of Materials in Civil Engineering*, vol. 12, 2019.

[16] Z. W. Z. Tao, "Finite element modelling of concrete-filled steel stub columns under axial compression," *Journal of Steel Construction*, vol. 89, pp. 121–131, 2013.

[17] U. Katwal, *Advanced Analysis of Steel-concrete Composite Frames*, Western Sydney University, Australia, 2018.

[18] Fib-bulletin-42, *Constitutive Modeling of High Strength/high Performance concrete*, International Federation for Structural Concrete, Lausanne, Switzerland, 2008.

[19] M. C. Fib, "Model Code 2010: final draft," *Fib Bulletin*, vol. 1, p. 66, 2012.

[20] N. D. Abaqus, "A material model for flexural crack simulation in reinforced concrete elements using ABAQUS,".